


 Cite this: *RSC Adv.*, 2019, **9**, 32232

The effects of Bi_2O_3 on the selective catalytic reduction of NO by propylene over Co_3O_4 nanoplates

 Dezhong Yu, ^a Xin Zhong, ^a Dong Liu ^{*a} and Ying Liang ^b

$\text{Bi}_2\text{O}_3/\text{Co}_3\text{O}_4$ catalysts prepared by the impregnation method were investigated for the selective catalytic reduction of NO by C_3H_6 (C_3H_6 -SCR) in the presence of O_2 . Their physicochemical properties were analyzed with SEM, XRD, H_2 -TPR, XPS, PL and IR measurements. It was found that the deposition of Bi_2O_3 on Co_3O_4 nanoplates enhanced the catalytic activity, especially at low reaction temperature. The SO_2 tolerance of Co_3O_4 in C_3H_6 -SCR activity was also improved with the addition of Bi_2O_3 . Among all catalysts tested, 10.0 wt% $\text{Bi}_2\text{O}_3/\text{Co}_3\text{O}_4$ achieved a 90% NO conversion at 200 °C with the total flow rate of 200 mL min^{-1} (GHSV 30 000 h^{-1}). No loss in its C_3H_6 -SCR activity was observed at different temperatures after the addition of 100 ppm of SO_2 to the reaction mixture. These enhanced catalytic behaviors may be associated with the improved oxidizing characteristics of 10.0 wt% $\text{Bi}_2\text{O}_3/\text{Co}_3\text{O}_4$. XRD results showed that Bi_2O_3 entered the lattice of Co_3O_4 , resulting in the formation of lattice distortion and structural defects. H_2 -TPR results showed that the reduction of Co_3O_4 was promoted and the diffusion of oxygen was accelerated with the addition of Bi_2O_3 . XPS measurements implied that more Co^{3+} formed on the 10.0% $\text{Bi}_2\text{O}_3/\text{Co}_3\text{O}_4$ catalysts. The improved oxidizing characteristics of the catalyst with the addition of Bi_2O_3 due to the synergistic effect of the nanostructure hybrid, thus enhanced the C_3H_6 -SCR reaction and hindered the oxidization of SO_2 . Therefore, the 10.0% $\text{Bi}_2\text{O}_3/\text{Co}_3\text{O}_4$ catalyst exhibited the highest NO conversion and strongest SO_2 tolerance ability.

Received 25th May 2019

Accepted 27th September 2019

DOI: 10.1039/c9ra03956b

rsc.li/rsc-advances

1 Introduction

Lean burn engines, which are generally used in gasoline and diesel powered vehicles, are more fuel-efficient than the stoichiometric gasoline engines.¹ They also effectively reduce unburned hydrocarbons, CO_2 and CO in exhausts.² However, lean burn engines operate with a large excess of air, leading to a significant concentration of oxygen in the exhausts, where the noble-metal three-way catalysts cannot work well to reduce nitrogen oxides (NO_x).³ A large amount of NO_x produced by lean burn engines leads to serious air pollution and public health problems.

In order to control NO_x emission under the lean burn conditions, selective catalytic reduction of NO by hydrocarbons (*e.g.* propylene) has been undertaken and reported in the literatures as one potential application (HC-SCR). Many classes of catalysts, including supported noble metals (*e.g.* Pt,^{4,5} Au^{6,7}), metal oxides (*e.g.* Ag_2O ,^{8,9} CuO ,^{10,11} SnO_2 ,¹²⁻¹⁴ CoO_x (ref. 15-18)) and zeolite types (ZSM-5,¹⁹ MCM-41 (ref. 20)) have been investigated. In general, the noble metals are active and stable even at lower temperature, but the formation of N_2O is undesirable by using

such precious metals, particularly, platinum-based catalysts. The zeolite-based catalysts were low thermal stability. Among metal oxides catalysts, cobalt oxides (*e.g.* Co_3O_4) are considered as one promising catalyst for HC-SCR due to its high catalytic activity.²¹ When combined with other oxides, such as CeO_2 ,¹⁶ ZrO_2 ,¹⁵ Al_2O_3 ,¹⁸ sulphated ZrO_2 ,²² the catalytic performances of the cobalt oxide catalyst could be improved as reported. These results implied that the chemical environment around cobalt oxide plays a crucial role in controlling the overall activity of cobalt containing catalysts in SCR reactions.

Bi_2O_3 , a common oxide semiconductor, is widely used in the fields of chemical engineering and electronics such as NO detection²³ and the oxidation or ammonoxidation of propylene.^{24,25} In the oxidation/ammonoxidation of propene over bismuth/molybdate catalyst, bismuth was thought to involve the rate-determining hydrogen abstraction from propylene,²⁶ exhibiting its mild oxidizing characteristics. This property might be also beneficial for the partial oxidation of propylene in C_3H_6 -SCR for NO reduction. Therefore, it is of considerable interest to explore the application of Bi_2O_3 in the reduction of NO with propylene.

In the present study, Co_3O_4 nanoplates and $\text{Bi}_2\text{O}_3/\text{Co}_3\text{O}_4$ were prepared with the solvothermal and impregnation method respectively. Their catalytic performances in the NO reduction by C_3H_6 in the presence of O_2 were investigated. The catalysts

^aSchool of Chemistry and Environmental Engineering, Wuhan Institute of Technology, Wuhan 430205, China. E-mail: witchem2018@163.com

^bSchool of Chemical Engineering, Hubei University of Arts and Science, Xiangyang 441053, China



were characterized with X-ray diffraction (XRD), temperature programmed reduction with hydrogen (H₂-TPR), and X-ray photoelectron spectra (XPS). The effects of Bi₂O₃ on the selective catalytic reduction of NO by propylene over Co₃O₄ nanoplates were expected to be elucidated.

2 Experimental

2.1 Preparation of Co₃O₄ and Bi₂O₃/Co₃O₄

The Co₃O₄ support was synthesized *via* the solvent-thermal method, 50 mmol CoCl₂ solution (200 mmol L⁻¹, Sinopharm Chemical Reagent Co. China) and 25 mL of NaOH (2 mol L⁻¹, Sinopharm Chemical Reagent Co. China) were added to a round-bottom flask, ultrasonicated for about 20 minutes to obtain a light brown uniform suspension. And then the suspension was transferred into a stainless steel autoclave with Teflon liner. The autoclave was sealed and maintained at 120 °C for 12 h. The obtained product was collected after washing with deionized water for several times, finally calcined at 500 °C for 5 h in air (S1).

The Bi₂O₃/Co₃O₄ catalysts with different Bi₂O₃ contents were synthesized by impregnation method as followed: 0.0155 g Bi(NO₃)₃·5H₂O and 20 mL 3% NH₃·H₂O were added into a round-bottom flask, ultrasonicated for about 20 minutes to obtain a white uniform suspension. After that, the Co₃O₄ support (S1) were added in the suspension, ultrasonicated for about 15 minutes to make it homogeneously distributed in the suspension. The suspension was then dried at 80 °C with continuous stirring for 1 h, further heated at 120 °C for 12 h followed by calcination at 500 °C in air for 4 h, yielding the 5.0 wt% Bi₂O₃/Co₃O₄ catalyst (S2). 10.0 wt% Bi₂O₃/Co₃O₄ (S3) and 15.0 wt% Bi₂O₃/Co₃O₄ (S4) were prepared with 0.0310 g and 0.0465 g Bi(NO₃)₃·5H₂O respectively. In addition, the physical mixture of 10% Bi₂O₃ nanoparticles and Co₃O₄ support was also prepared and labeled as S5. As references, classical catalysts 4% Ag/Al₂O₃ and 2% Pt/Al₂O₃ were prepared to compare the catalytic performance of the Bi₂O₃/Co₃O₄ catalysts.

2.2 Catalytic activity tests

C₃H₆-SCR over the catalysts was carried out at atmospheric pressure in a fixed-bed quartz reactor (diameter = 10 mm). 0.1 g catalyst was used in each run with a reaction mixture composed of 200 ppm NO, 200 ppm C₃H₆, 100 ppm SO₂ (when needed) and 10 vol% O₂ in balance gas N₂. The total flow rate was 200 mL min⁻¹, corresponding to a GHSV 30 000 h⁻¹. Reaction temperature ranges from 100 to 500 °C. The concentration of NO was continuously measured by a NO analyzer (Thermo Environmental Instruments Inc., model 42c), which monitors NO, NO₂, and NO_x (NO_x represents NO + NO₂). The removal efficiency of NO was calculated as NO removal (%) = (1 - C/C₀) × 100%, where C and C₀ are concentrations of NO in the outlet and inlet, respectively.

2.3 Catalysts characterization

Scanning electron microscopy (SEM) images were taken on a Hitachi S4800 scanning electron microscope operating at 5.0 kV. X-ray powder diffraction (XRD) was carried out on

Brukeraxs D8 Discover (Cu K α = 1.5406 Å). The scanning rate is 1° min⁻¹ in the 2 θ range from 20 to 80 degree. The reducibility of Bi₂O₃/Co₃O₄ catalysts was estimated by temperature programmed reduction with hydrogen analysis (H₂-TPR). The experiments were carried out with a Micromeritics 2910 apparatus using H₂/Ar (3/97, v/v) gas with a total flow rate of 15 mL min⁻¹. In each run, 0.030 g of the catalyst was previously activated at 500 °C for 30 min under air, and then cooled to RT. TPR started with the introduction of the mixture of H₂ and Ar. The catalyst was heated from room temperature (RT) to 1000 °C (10 °C min⁻¹). H₂ consumption was continuously monitored with the thermal conductivity detector. X-ray photoelectron spectra (XPS) of the catalysts were measured in a VG Multilab 2000 spectrometer by using Al K α (1486.6 eV) radiation as the X-ray source. Photoluminescence (PL) measurement was carried out on a Shimadzu RF-5301 PC fluorescence spectrophotometer. Raman spectra were recorded using a Horiba Jobin-Yvon Lab Ram HR800 Raman microspectrometer, with an excitation laser at 514 nm.

3 Results

3.1 Scanning electron microscope (SEM) observation and XRD analysis

Co₃O₄ nanoplates with different dimensions were observed on the support Co₃O₄ (S1), shown in Fig. 1(a). Fig. 1(b-d) presented Bi₂O₃/Co₃O₄ catalysts with different Bi₂O₃ loading amounts. It was shown that Bi₂O₃ nanoparticles with dimension *ca.* 20 nm were supported on Co₃O₄. And the crystal size of Bi₂O₃ slightly increased with increasing Bi₂O₃ loading amount from 5% to 15%.

Fig. 2(A) shows the XRD patterns of the synthesized Co₃O₄ and Bi₂O₃/Co₃O₄ catalysts. It can be seen that the Co₃O₄ support possessed the characteristic peaks of Co₃O₄ (JCPDS 73-1701, *a* = 5.45 Å). Besides the characteristic peaks of Co₃O₄, the diffraction peaks due to Bi₂O₃ (JCPDS 22-515, *a* = 10.94 Å and *c* = 11.28 Å) were also observed on Bi₂O₃/Co₃O₄ catalysts which became sharper with the increase of Bi₂O₃ loading amount. It was suggested that the crystal size of Bi₂O₃ was bigger on the catalyst with higher loading amount of Bi₂O₃, which was consistent with the SEM observations. Moreover, the diffraction peaks of Co₃O₄ over Bi₂O₃/Co₃O₄ catalysts behaved a slight shift towards lower degree in comparison with that of Co₃O₄, shown in Fig. 2(B). It indicated that the Bi³⁺ inserted the lattice of Co₃O₄ in the preparation process, and changed the lattice parameter of Co₃O₄ due to the different radius of Bi and Co atoms. At the same time, the characteristic peak of Co₃O₄ became weak obviously after the deposition of Bi₂O₃, which revealed the reduction of crystal size. It was implied that the insertion of Bi₂O₃ induced the structure defect of Co₃O₄ and suppressed the growth of crystal.

3.2 Temperature-programmed reduction by hydrogen (H₂-TPR)

The H₂-TPR profiles of Co₃O₄, Bi₂O₃ and Bi₂O₃/Co₃O₄ catalysts were shown in Fig. 3. For the reduction of Bi₂O₃, a sharp peak

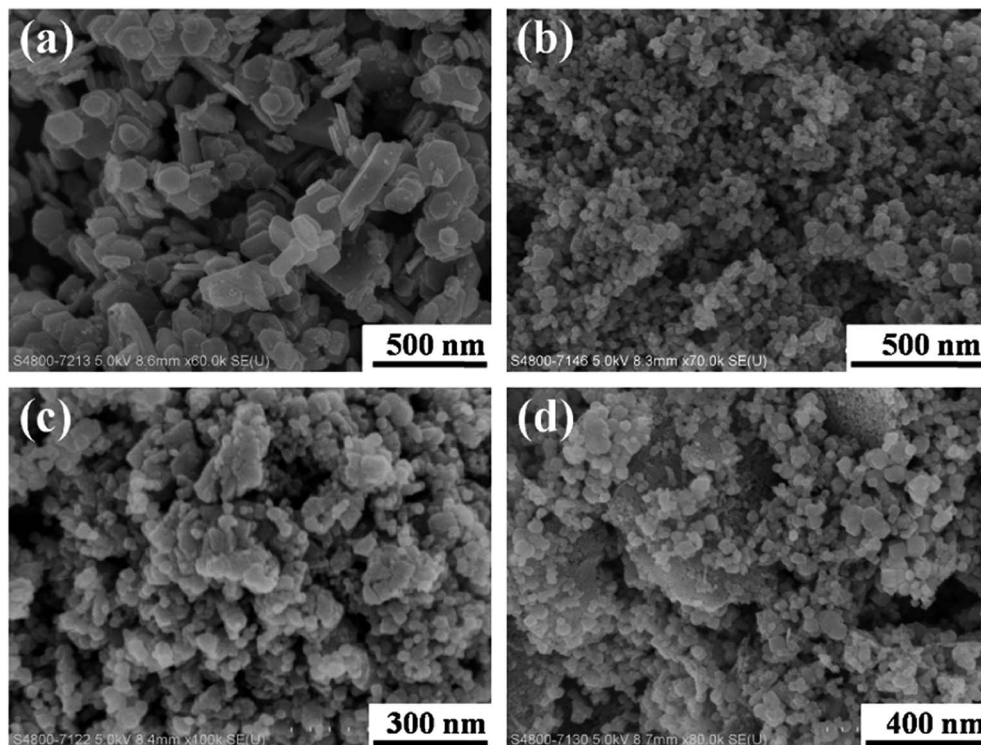


Fig. 1 SEM images of Co_3O_4 (a), 5.0% $\text{Bi}_2\text{O}_3/\text{Co}_3\text{O}_4$ (b), 10.0% $\text{Bi}_2\text{O}_3/\text{Co}_3\text{O}_4$ (c) and 15.0% $\text{Bi}_2\text{O}_3/\text{Co}_3\text{O}_4$ (d).

was observed at *ca.* 490 °C, implying the reduction of Bi^{3+} in a narrow temperature range. A broad reduction peak from 330 to 460 °C with a large shoulder at the lower reduction temperature (*ca.* 380 °C) appeared on Co_3O_4 support (S1). Many researchers reported that the reduction of Co_3O_4 was a two-step reduction process involving the intermediate reduction of CoO .^{16,21,27} Two main clear reduction peaks respectively located around 186 °C and 310–480 °C were shown in the TPR spectra. The low temperature TPR peak was associated with the reduction of Co^{3+} to Co^{2+} , and the peak at high temperature was the subsequent reduction of CoO to metallic cobalt. In the TPR spectrum of Co_3O_4 synthesized in the present work, there are no obvious two peaks probably due to an abroad particle size distribution as shown in SEM observation. The large shoulder at 376 °C (peak I) in Fig. 3 should be attributed to the reduction of Co^{3+} to Co^{2+} , and main reduction peak (peak II) is ascribed to the reduction of CoO to metallic cobalt.

The reduction process of $\text{Bi}_2\text{O}_3/\text{Co}_3\text{O}_4$ catalysts (S2–S4) became complicated with the introduction of Bi_2O_3 . The reduction peak at 487 °C became wider and shifted towards to the lower temperature, especially on the $\text{Bi}_2\text{O}_3/\text{Co}_3\text{O}_4$ catalyst with the highest Bi loading amount (S4). In addition, two new peaks around 342 °C (peak I) and 402 °C (peak II) respectively ascribed to the reduction of Co^{3+} to Co^{2+} , Co^{2+} to metallic Co appeared on $\text{Bi}_2\text{O}_3/\text{Co}_3\text{O}_4$ catalysts (S2–S4).²⁸ Compared with the bulk Co_3O_4 (S1), both the reduction peak of Co^{3+} and that of Co^{2+} shifted to lower temperature after the deposition of Bi_2O_3 , implying the promoted reduction of Co_3O_4 . Moreover, the larger reduction peak I than peak II on S2–S4 samples indicated that

the ratio of $\text{Co}^{3+}/\text{Co}^{2+}$ was higher on S2–S4 samples than that on the Co_3O_4 (S1). It revealed that the deposition of Bi_2O_3 on Co_3O_4 affected the oxidized state of cobalt in the synthesized Co_3O_4 , more Co^{3+} were present on the supported samples (S2–S4) than the pure Co_3O_4 .

3.3 X-ray photoelectron spectroscopy (XPS)

XPS measurements were carried out on Co_3O_4 and 10.0% $\text{Bi}_2\text{O}_3/\text{Co}_3\text{O}_4$ catalysts to examine the influence of Bi_2O_3 on the surface electronic state of Co_3O_4 . The Co 2p and O 1s XPS profiles are shown in Fig. 4. In the Co 2p (Fig. 7(a)), the main peaks located at 779.6–781.3 eV and 794.8–796.5 eV are ascribed to $\text{Co 2p}_{1/2}$ and $\text{Co 2p}_{3/2}$ spin-orbital peaks, respectively.^{29,30} It was well-known that the spin-orbit splitting value for Co^{3+} compounds is 15.0 eV, 15.1–15.3 eV for the mixed-valence Co_3O_4 . Here, the spin-orbit splitting values of Co 2p for Co_3O_4 and 10.0% $\text{Bi}_2\text{O}_3/\text{Co}_3\text{O}_4$ are the same, 15.2 eV, which is close to that of mixed-valence Co_3O_4 . So the cobalt species on both S1 and S3 should be Co_3O_4 , agreeable with the XRD and TPR results.

Based on the restriction that $\text{Co 2p}_{3/2}$ binding energies of Co^{2+} and Co^{3+} components are 781.3 eV and 779.6 eV, respectively, the spin-orbit doublet splitting is 15.2 eV with a fixed ratio of 2/1 for the $2\text{p}_{3/2}$ -to- $2\text{p}_{1/2}$ peak area,²⁹ the Co 2p spectra of S1 and S3 can be fitted to the Co^{2+} (peak II and IV) and Co^{3+} (peak I and III) components.^{30,31} The satellite peak of Co^{2+} and that of Co^{3+} in Co_3O_4 were also respectively observed at 787.0 eV and 791.0 eV.^{32,33} Fig. 4 shows that the peak areas of peak I and III increased with the addition of Bi_2O_3 , implying that the surface Co^{3+} and the surface content ratio of $\text{Co}^{3+}/\text{Co}^{2+}$

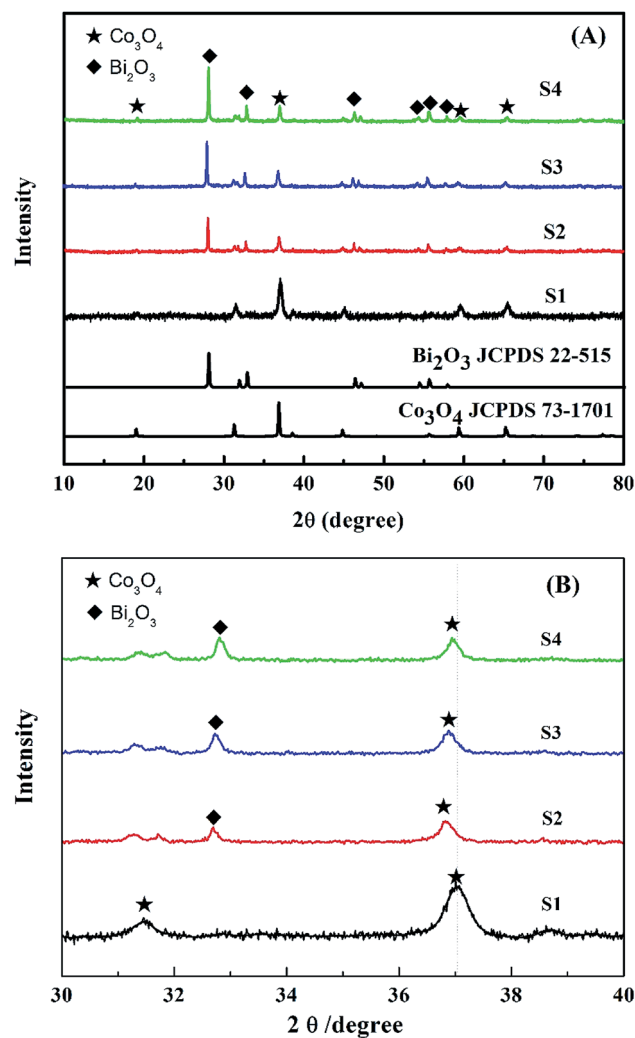


Fig. 2 XRD patterns of Co_3O_4 (S1), 5.0% $\text{Bi}_2\text{O}_3/\text{Co}_3\text{O}_4$ (S2), 10.0% $\text{Bi}_2\text{O}_3/\text{Co}_3\text{O}_4$ (S3) and 15.0% $\text{Bi}_2\text{O}_3/\text{Co}_3\text{O}_4$ (S4) in the wide (A) and narrow (B) ranges.

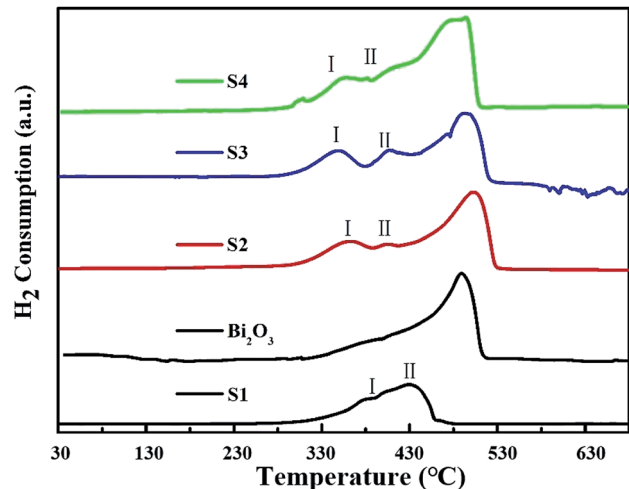


Fig. 3 H_2 -TPR profiles of pure Co_3O_4 (S1), Bi_2O_3 , 5.0% $\text{Bi}_2\text{O}_3/\text{Co}_3\text{O}_4$ (S2), 10.0% $\text{Bi}_2\text{O}_3/\text{Co}_3\text{O}_4$ (S3) and 15.0% $\text{Bi}_2\text{O}_3/\text{Co}_3\text{O}_4$ (S4).

increased with the addition of Bi_2O_3 . More Co^{3+} was present on 10.0% $\text{Bi}_2\text{O}_3/\text{Co}_3\text{O}_4$ (S3) than the bulk Co_3O_4 support (S1), as consistent with the TPR results.

The O 1s XPS spectra of Co_3O_4 and $\text{Bi}_2\text{O}_3/\text{Co}_3\text{O}_4$ catalysts are shown in Fig. 4(b). For the Co_3O_4 sample, there are two peaks (I and II). The peak I located at ~ 530.1 eV is attributed to the surface lattice of Co_3O_4 , and the peak II at ~ 531.5 eV is associated with OH^- groups.³⁴ In the case of 10.0% $\text{Bi}_2\text{O}_3/\text{Co}_3\text{O}_4$, besides the peak I and II, one new peak at ~ 532.8 eV appeared, which should be related to the contribution of the oxygen from Bi_2O_3 .

3.4 Photoluminescence (PL) and Raman spectra

PL emission spectra originating from the recombination of free charge carriers are useful to reveal the migration, transfer and separation of photogenerated charge carriers. Fig. 5 shows photoluminescence emission spectra of different catalysts at room temperature. All samples show one luminescence peak center at about 358 nm, which can be attributed to the radiative recombination of charge carriers. The pure Co_3O_4 has the strongest PL emission peak. This charge recombination process of Co_3O_4 can be greatly inhibited by the deposition of Bi_2O_3 on

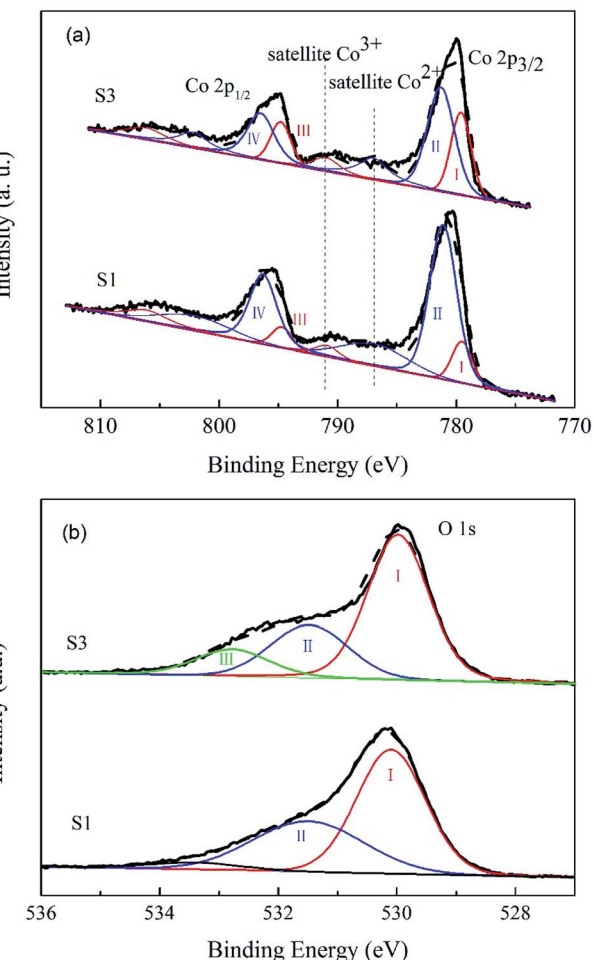


Fig. 4 XPS study of Co_3O_4 (S1) and 10.0% $\text{Bi}_2\text{O}_3/\text{Co}_3\text{O}_4$ (S3): (a) Co 2p spectra, (b) O 1s spectra.

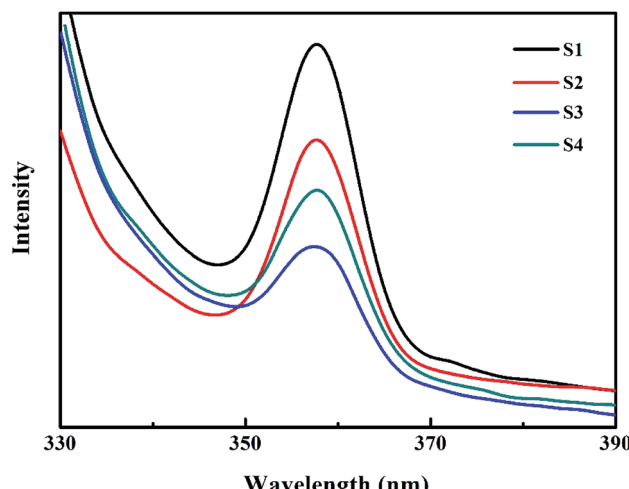


Fig. 5 Room-temperature PL spectra of Co_3O_4 (S1), 5.0% $\text{Bi}_2\text{O}_3/\text{Co}_3\text{O}_4$ (S2), 10.0% $\text{Bi}_2\text{O}_3/\text{Co}_3\text{O}_4$ (S3) and 15.0% $\text{Bi}_2\text{O}_3/\text{Co}_3\text{O}_4$ (S4).

Co_3O_4 , 10.0% $\text{Bi}_2\text{O}_3/\text{Co}_3\text{O}_4$ (S3) has the lowest PL emission peak, which is associated with its structural imperfection. The structural imperfection originating from the insertion of the Bi^{3+} into the lattice of Co_3O_4 , as evidenced by XRD, increased the number of structural defects (e.g., oxygen vacancies), which could capture the electrons or holes, thus resulting in low radiative PL emission.

Fig. 6 shows the Raman spectra of 10.0% $\text{Bi}_2\text{O}_3/\text{Co}_3\text{O}_4$ (S3), pure Co_3O_4 (S1) and Bi_2O_3 . For the pure Co_3O_4 , the Raman peak at 655 cm^{-1} was corresponded to the symmetry of Co_3O_4 .³⁵ 10.0% $\text{Bi}_2\text{O}_3/\text{Co}_3\text{O}_4$ gave the similar Raman spectra with Co_3O_4 , while the characteristic peaks of Bi_2O_3 could not be detected. Compared with Co_3O_4 , the Raman peaks on 10.0% $\text{Bi}_2\text{O}_3/\text{Co}_3\text{O}_4$ shifted to the lower frequencies with stronger intensities, which associated with the lattice distortion or residual stress of the spinel structure. The XRD results showed that part of Bi_2O_3 entered the lattice of Co_3O_4 over 10.0% $\text{Bi}_2\text{O}_3/\text{Co}_3\text{O}_4$, leading to

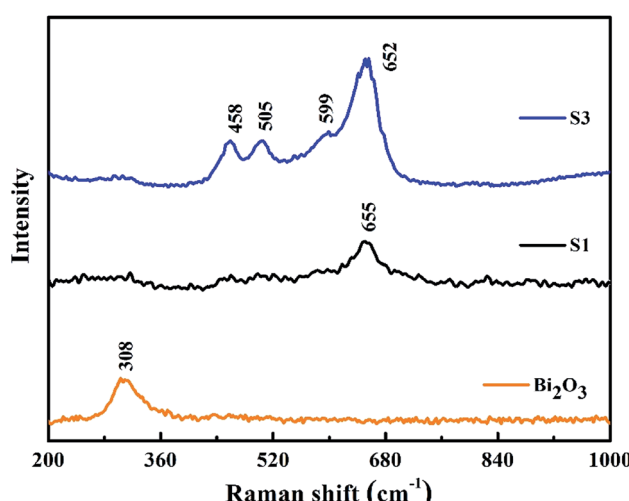


Fig. 6 Raman spectra of Co_3O_4 (S1) and 10.0% $\text{Bi}_2\text{O}_3/\text{Co}_3\text{O}_4$ (S3).

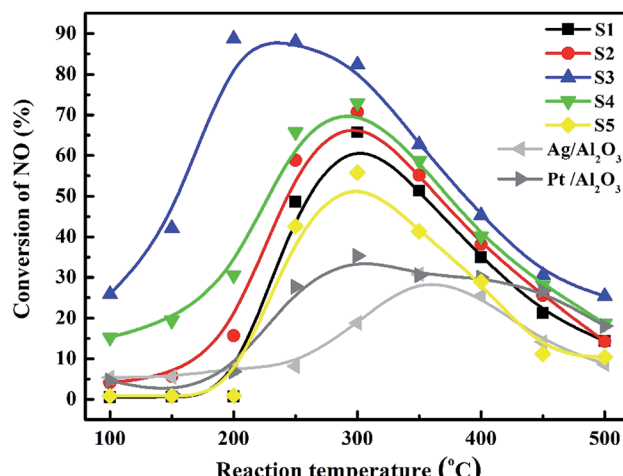


Fig. 7 NO conversions over the catalysts: S1: Co_3O_4 ; S2: 5.0% $\text{Bi}_2\text{O}_3/\text{Co}_3\text{O}_4$; S3: 10.0% $\text{Bi}_2\text{O}_3/\text{Co}_3\text{O}_4$; S4: 15.0% $\text{Bi}_2\text{O}_3/\text{Co}_3\text{O}_4$; S5: the physical mixture of Bi_2O_3 and Co_3O_4 .

the lattice distortion and lattice defect. The highly defective structure formed on 10.0% $\text{Bi}_2\text{O}_3/\text{Co}_3\text{O}_4$ could accelerate the adsorption and activation of O_2 , which was suggested to be related to the better catalytic performance.

3.5 Catalytic performance

Fig. 7 depicted the NO conversions over the $\text{Bi}_2\text{O}_3/\text{Co}_3\text{O}_4$ catalysts with different Bi_2O_3 contents (S1–S4), the physical mixture of 10% Bi_2O_3 nanoparticles and Co_3O_4 support (S5), 4% $\text{Ag}/\text{Al}_2\text{O}_3$ and 2% $\text{Pt}/\text{Al}_2\text{O}_3$ reference catalysts within the reaction temperature range of 100–500 °C. Co_3O_4 and $\text{Bi}_2\text{O}_3/\text{Co}_3\text{O}_4$ catalysts showed higher NO reduction activity than those of $\text{Ag}/\text{Al}_2\text{O}_3$ and $\text{Pt}/\text{Al}_2\text{O}_3$, especially $\text{Bi}_2\text{O}_3/\text{Co}_3\text{O}_4$ catalysts. The conversion of NO over Co_3O_4 support (S1) firstly increased with reaction temperature, reached the maximum conversion (*ca.* 60%) at *ca.* 300 °C and then decreased at higher temperature. The NO conversion was further increased with the addition of Bi_2O_3 into Co_3O_4 with the activity order: Co_3O_4 (S1) < 5.0% $\text{Bi}_2\text{O}_3/\text{Co}_3\text{O}_4$ (S2) < 15.0% $\text{Bi}_2\text{O}_3/\text{Co}_3\text{O}_4$ (S4) < 10.0% $\text{Bi}_2\text{O}_3/\text{Co}_3\text{O}_4$ (S3). Among all catalysts tested, 10.0% $\text{Bi}_2\text{O}_3/\text{Co}_3\text{O}_4$ (S3) possessed the highest activity for NO conversion in the reaction temperature window, reaching *ca.* 90% NO conversion at 200 °C. NO conversion under the lower reaction temperature (100–250 °C) over S3 also reached the highest among the catalysts tested. In contrast, the mixture of 10% Bi_2O_3 nanoparticles and Co_3O_4 support (S5) showed lower activity than S1 and S3. It was indicated that the interaction between Bi_2O_3 and Co_3O_4 in S3 is not the simply physical mixture like S5. The chemical interaction between them took place in S3 and should contribute the admirable catalytic performance of S3 in the C_3H_6 -SCR reaction.

SO_2 usually exists in the diesel engine exhaust. So it is necessary to investigate the SO_2 tolerance of the catalyst in C_3H_6 -SCR. Fig. 8 exhibited the effects of 100 ppm SO_2 co-fed in the reaction gas on the NO conversions over the catalysts at the different reaction temperatures. NO conversion over the S3

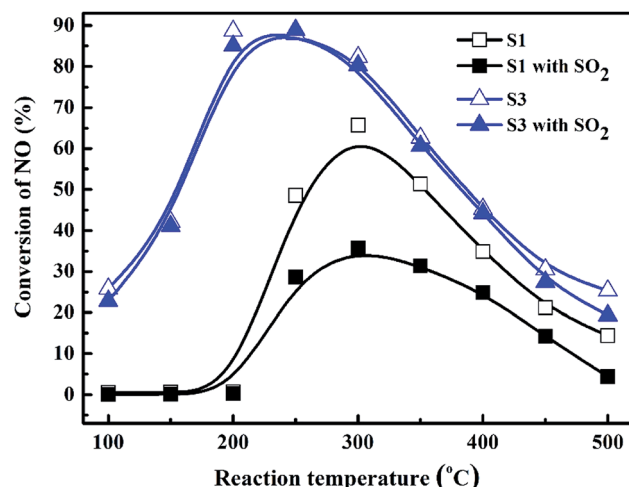


Fig. 8 SO_2 resistibilities of Co_3O_4 (S1) and 10.0% $\text{Bi}_2\text{O}_3/\text{Co}_3\text{O}_4$ (S3) with the reaction temperature.

(10% $\text{Bi}_2\text{O}_3/\text{Co}_3\text{O}_4$) catalyst clearly did not change in the wide reaction window. The steady-state NO conversion reached 90.3% on S3 at 250 °C in the presence and absence of SO_2 . In contrast, NO conversion decreased from 65.8% to 35.7% at 300 °C on the Co_3O_4 support (S1) when 100 ppm SO_2 was contained in the feed gas. NO conversions at other reaction temperatures also reduced in the presence of SO_2 . These results obviously suggested that 10% $\text{Bi}_2\text{O}_3/\text{Co}_3\text{O}_4$ exhibited good resistibility against SO_2 that coexists with NO and C_3H_6 in the reaction mixture.

Fig. 9 shows the SO_2 durability of 10% $\text{Bi}_2\text{O}_3/\text{Co}_3\text{O}_4$ catalyst with the reaction time at the optimum reaction temperature 200 °C in the C_3H_6 -SCR of NO. When NO conversion reached to the maximum (89.3%), 100 ppm SO_2 was added in the reaction system, NO conversion immediately decreased. It was probably due to the competitive adsorption of NO and SO_2 on the active site. 20 min later, NO conversion reduced to 63.6%. After that,

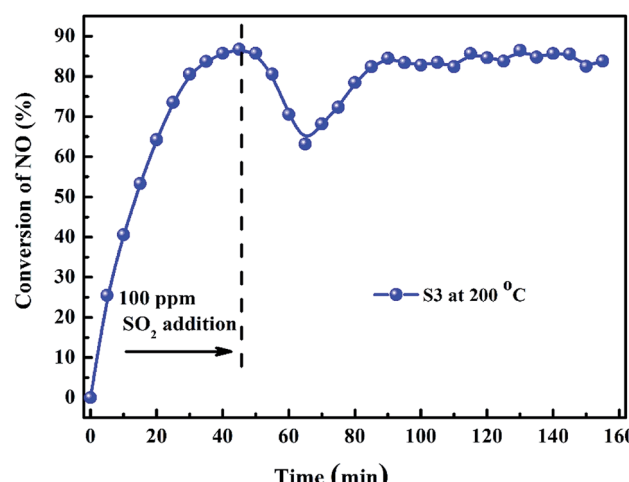


Fig. 9 NO conversion over 10.0% $\text{Bi}_2\text{O}_3/\text{Co}_3\text{O}_4$ (S3) before and after the addition of SO_2 (reaction temperature: 200 °C).

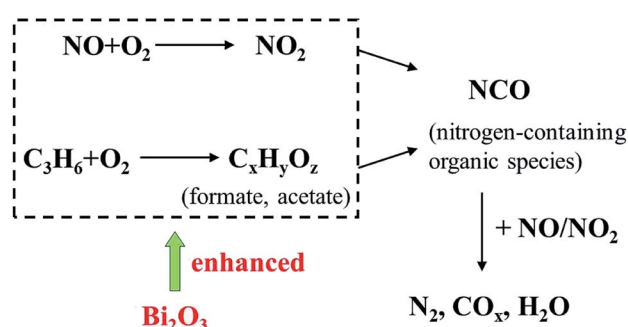
NO conversion recovered to 85.7%, and maintained at *ca.* 88% through the whole reaction period of 90 min. This result further illustrates the outstanding SO_2 resistibility of 10% $\text{Bi}_2\text{O}_3/\text{Co}_3\text{O}_4$ in the long time-reaction.

4 Discussions

In this study, the deposition of Bi_2O_3 with the proper loading amount on Co_3O_4 nanoplates enhanced NO conversion over Co_3O_4 , especially at low reaction temperature (<200 °C). 10.0% $\text{Bi}_2\text{O}_3/\text{Co}_3\text{O}_4$ catalyst also showed the strong resistibility against SO_2 in the feed gas. XRD results showed Bi_2O_3 could enter the lattice of Co_3O_4 , and promote the formation of the lattice distortion and structural defect as demonstrated by PL spectra and IR spectra. The H_2 -TPR and XPS results showed that more Co^{3+} appeared with the deposition of Bi_2O_3 . These changes were probably related to the promotive effects of Bi_2O_3 in the C_3H_6 -SCR reaction.

Scheme 1 illustrated the mechanistic investigations for the HC-SCR reactions in the previous literatures.^{17,36,37} According to these findings, the reactants (C_3H_6 , NO and NO_2) are supposed to be first adsorbed on the active sites over the catalyst surface. Subsequently, the adsorbed nitrates formed *via* NO oxidation by O_2 . C_3H_6 was also activated to form $\text{C}_x\text{H}_y\text{O}_z$ species such as formate, acetate and so on. As these $\text{C}_x\text{H}_y\text{O}_z$ species become available, nitrates subsequently reacted with them to yield nitrogen-containing organic species, such as NCO species. The final step would be the interaction of NOC intermediates with NO_x (NO , NO_x), decomposing into N_2 , CO_x and H_2O as final products. This proposed reaction process reveals the crucial role of O_2 in the feed gas and the importance of oxidizing characteristics of the catalyst surface.

In our work, PL and IR results showed that more oxygen vacancies were produced on the Co_3O_4 after the doping of Bi_2O_3 . The vacancy could accelerate the adsorption, activation and diffusion of oxygen, which was suggested to be available for the oxidation reactions involved in HC-SCR. The doped Bi_2O_3 also increased the Co^{3+} concentration on the surface. The richness of Co^{3+} could promote the adsorption and activation of NO and (or) C_3H_6 . What is more is the mild oxidizing characteristics of



$\text{Bi}_2\text{O}_3/\text{Co}_3\text{O}_4$ showed high NO conversion and strong SO_2 tolerance.

Scheme 1 The promotive effects of Bi_2O_3 on NO reduction by propane over Co_3O_4 catalyst.

bismuth oxide in the selective oxidation and ammonoxidation of propene to acrolein and acrylonitrile. It will accelerate the formation of $C_xH_yO_z$ species. In short, the addition of Bi_2O_3 into the Co_3O_4 in the present study probably influenced the oxidation process in the C_3H_6 -SCR reaction, favored the activation of C_3H_6 and NO, and then enhanced the following NCO intermediate formation and its decomposition with reaction with NO_x to N₂.

About poisoning HC-SCR catalyst with SO₂, the previous studies reported that the suppression effect of SO₂ on the SCR catalyst could be attributed to the formation of sulphate on the catalyst.³⁸ The presence of surface SO₄²⁻ groups blocked the formation of nitrate and decreased the amount of adsorbed nitrates. Thus it hindered the transformation of NOC species and decreased the catalytic activity. In our work, the presence of 100 ppm SO₂ in the feed gas decreased the NO conversion over Co_3O_4 catalyst, while the SO₂ tolerance of Bi_2O_3/Co_3O_4 was strong. 10% Bi_2O_3/Co_3O_4 showed the good stability when SO₂ was co-fed in the mixture gas during 90 min. This promotive role of Bi_2O_3 on the resistibility against SO₂ also could be explained by the oxidizing properties of 10% Bi_2O_3/Co_3O_4 . The addition of Bi_2O_3 into Co_3O_4 promoted the partial oxidation of propene activation of C_3H_6 . The activation of C_3H_6 over 10% Bi_2O_3/Co_3O_4 seems more competitive in the comparison with the oxidization of SO₂ to form surface sulfate. Subsequently, it is suggested that the addition of Bi_2O_3 into Co_3O_4 is one appropriate method for improving the SO₂ resistance of Co_3O_4 .

5 Conclusions

The optimum Bi_2O_3 loading on the Co_3O_4 nanoplates for the C_3H_6 -SCR of NO was about 10%, giving the best catalytic activity, especially at low reaction temperature, as well as the strongest SO₂ tolerance. The decoration of moderate Bi_2O_3 on Co_3O_4 influenced the oxidation state of Co_3O_4 , facilitate the surface oxygen mobility and the partial oxidation of propene involved in the C_3H_6 -SCR reaction. Therefore, the combination of Co_3O_4 with Bi_2O_3 is more active than Co_3O_4 . The addition of 100 ppm SO₂ to the feed hardly affected the catalytic performance of 10% Bi_2O_3/Co_3O_4 .

Conflicts of interest

There are no conflict to declare.

Acknowledgements

This work was supported by the China National Natural Science Foundation (No. 51178360) and Hubei Superior and Distinctive Discipline Group of "Mechatronics and Automobiles" (XKQ2019058).

References

- 1 C. R. Thomas, J. A. Pihl, M. J. Lance, T. J. Toops, J. E. Parks and J. Lauterbach, Effects of four-mode hydrothermal aging on three-way catalysts for passive selective catalytic reduction to control emissions from lean-burn gasoline engine, *Appl. Catal., B*, 2019, **244**, 284–294.
- 2 Y. Rui, M. Ming, Z. Jing, L. Zheng, T. Hu and X. Li, A noble-metal-free SCR-LNT coupled catalytic system used for high-concentration NO_x reduction under lean-burn condition, *Catal. Today*, 2018, **347**, 347–356.
- 3 J. A. Lupescu, J. W. Schwank, G. B. Fisher, J. Hangas, S. L. Peczonczyk and W. A. Paxton, Pd model catalysts: effect of air pulse length during redox aging on Pd redispersion, *Appl. Catal., B*, 2018, **223**, 76–90.
- 4 Y. Hu and K. Griffiths, Selective Catalytic Reduction of NO by Hydrocarbons on a Stepped Pt Surface: Influence of SO₂ and O₂, *J. Phys. Chem. C*, 2015, **119**, 19789–19801.
- 5 M. Khosravi, C. Sola, A. Abedi, R. E. Hayes, W. S. Epling and M. Votsmeier, Oxidation and selective catalytic reduction of NO by propene over Pt and Pt:Pd diesel oxidation catalysts, *Appl. Catal., B*, 2014, **147**, 264–274.
- 6 P. Miquel, P. Granger, N. Jagtap, S. Umbarkar, M. Dongare and C. Dujardin, NO reduction under diesel exhaust conditions over Au/Al₂O₃ prepared by deposition-precipitation method, *J. Mol. Catal. A: Chem.*, 2010, **322**, 90–97.
- 7 X. Wang, N. Maeda and A. Baiker, Synergistic Effects of Au and FeO_x Nanocomposites in Catalytic NO Reduction with CO, *ACS Catal.*, 2016, **6**, 7898–7906.
- 8 P. A. Kumar, M. P. Reddy, B. Hyun-Sook and H. H. Phil, Influence of Mg Addition on the Catalytic Activity of Alumina Supported Ag for C_3H_6 -SCR of NO, *Catal. Lett.*, 2009, **131**, 85–97.
- 9 A. Musi, P. Massiani, D. Brouri, J.-M. Trichard and P. Da Costa, On the Characterisation of Silver Species for SCR of NO_x with Ethanol, *Catal. Lett.*, 2008, **128**, 25–30.
- 10 P. Namkhang and P. Kongkachuchay, Synthesis of Copper-Based Nanostructured Catalysts on SiO₂–Al₂O₃, SiO₂–TiO₂, and SiO₂–ZrO₂ Supports for NO Reduction, *J. Nanosci. Nanotechnol.*, 2015, **15**, 5410–5417.
- 11 J. Liu, X. Li, Q. Zhao, D. Zhang and P. Ndokoye, The selective catalytic reduction of NO with propene over Cu-supported Ti–Ce mixed oxide catalysts: promotional effect of ceria, *J. Mol. Catal. A: Chem.*, 2013, **378**, 115–123.
- 12 Z. Liu, J. Li and J. Hao, Selective catalytic reduction of NO_x with propene over SnO₂/Al₂O₃ catalyst, *Chem. Eng. J.*, 2010, **165**, 420–425.
- 13 M. Chen, J. Yang, Y. Liu, W. Li, J. Fan, X. Ran, W. Teng, Y. Sun, W.-x. Zhang, G. Li, S. X. Dou and D. Zhao, TiO₂ interpenetrating networks decorated with SnO₂ nanocrystals: enhanced activity of selective catalytic reduction of NO with NH₃, *J. Mater. Chem. A*, 2015, **3**, 1405–1409.
- 14 L. Zhang, L. Li, Y. Cao, Y. Xiong, S. Wu, J. Sun, C. Tang, F. Gao and L. Dong, Promotional effect of doping SnO₂ into TiO₂ over a CeO₂/TiO₂ catalyst for selective catalytic reduction of NO by NH₃, *Catal. Sci. Technol.*, 2015, **5**, 2188–2196.
- 15 D. Pietrogiacomi, M. C. Campa, L. R. Carbone, S. Tuti and M. Occhiuzzi, N₂O decomposition on CoO_x, CuO_x, FeO_x or MnO_x supported on ZrO₂: the effect of zirconia doping



with sulfates or K^+ on catalytic activity, *Appl. Catal., B*, 2016, **187**, 218–227.

16 Y. Yu, Q. Zhong, W. Cai and J. Ding, Promotional effect of N-doped CeO_2 supported CoO_x catalysts with enhanced catalytic activity on NO oxidation, *J. Mol. Catal. A: Chem.*, 2015, **398**, 344–352.

17 F. Huang, W. Hu, J. Chen, Y. Wu, P. Qu, S. Yuan, L. Zhong and Y. Chen, Insight into Enhancement of NO Reduction with Methane by Multifunctional Catalysis over a Mixture of Ce/HZSM-5 and CoO_x in Excess of Oxygen, *Ind. Eng. Chem. Res.*, 2018, **57**, 13312–13317.

18 L. Zhang, X. Yao, Y. Lu, C. Sun, C. Tang, F. Gao and L. Dong, Effect of precursors on the structure and activity of CuO – CoO_x /gamma-Al₂O₃ catalysts for NO reduction by CO, *J. Colloid Interface Sci.*, 2018, **509**, 334–345.

19 B. Dou, G. Lv, C. Wang, Q. Hao and K. Hui, Cerium doped copper/ZSM-5 catalysts used for the selective catalytic reduction of nitrogen oxide with ammonia, *Chem. Eng. J.*, 2015, **270**, 549–556.

20 M. Sakmeche, A. Belhakem, R. Kessas and S. A. Ghomari, Effect of parameters on NO reduction by methane in presence of excess O₂ and functionalized AlMCM-41 as catalysts, *J. Taiwan Inst. Chem. Eng.*, 2017, **80**, 333–341.

21 F. Bin, C. Song, G. Lv, J. Song, X. Cao, H. Pang and K. Wang, Structural Characterization and Selective Catalytic Reduction of Nitrogen Oxides with Ammonia: A Comparison between Co/ZSM-5 and Co/SBA-15, *J. Phys. Chem. C*, 2012, **116**, 26262–26274.

22 D. Pietrogiacomi, A. Magliano, P. Ciambelli, D. Sannino, M. C. Campa and V. Indovina, The effect of sulphation on the catalytic activity of CoO_x /ZrO₂ for NO reduction with NH₃ in the presence of O₂, *Appl. Catal., B*, 2009, **89**, 33–40.

23 A. Cabot, A. Marsal, J. Arbiol and J. R. Morante, Bi₂O₃ as a selective sensing material for NO detection, *Sens. Actuators, B*, 2004, **99**, 74–89.

24 J. F. Brazdil, M. A. Toft, S. S. Y. Lin, S. T. McKenna, G. Zajac, J. A. Kaduk and J. T. Golab, Characterization of bismuth-cerium-molybdate selective propylene ammoxidation catalysts, *Appl. Catal., A*, 2015, **495**, 115–123.

25 Y.-H. Lei and Z.-X. Chen, Theoretical study of propene oxidation on Bi₂O₃ surfaces, *Sci. China: Chem.*, 2015, **58**, 593–600.

26 R. B. Licht and A. T. Bell, A DFT Investigation of the Mechanism of Propene Ammoxidation over α -Bismuth Molybdate, *ACS Catal.*, 2016, **7**, 161–176.

27 S. Kumar Megarajan, S. Rayalu, Y. Teraoka and N. Labhsetwar, High NO oxidation catalytic activity on non-noble metal based cobalt-ceria catalyst for diesel soot oxidation, *J. Mol. Catal. A: Chem.*, 2014, **385**, 112–118.

28 J.-W. Shi, G. Gao, Z. Fan, C. Gao, B. Wang, Y. Wang, Z. Li, C. He and C. Niu, $Ni_yCo_{1-y}Mn_2O_x$ microspheres for the selective catalytic reduction of NO_x with NH₃: the synergetic effects between Ni and Co for improving low-temperature catalytic performance, *Appl. Catal., A*, 2018, **560**, 1–11.

29 D. Wang, Q. Wang and T. Wang, Morphology-controllable synthesis of cobalt oxalates and their conversion to mesoporous Co₃O₄ nanostructures for application in supercapacitors, *Inorg. Chem.*, 2011, **50**, 6482–6492.

30 J.-W. Shi, Z. Fan, C. Gao, G. Gao, B. Wang, Y. Wang, C. He and C. Niu, Mn–Co Mixed Oxide Nanosheets Vertically Anchored on H₂Ti₃O₇ Nanowires: Full Exposure of Active Components Results in Significantly Enhanced Catalytic Performance, *ChemCatChem*, 2018, **10**, 2833–2844.

31 Z. Zhu, G. Lu, Z. Zhang, Y. Guo, Y. Guo and Y. Wang, Highly Active and Stable Co₃O₄/ZSM-5 Catalyst for Propane Oxidation: Effect of the Preparation Method, *ACS Catal.*, 2013, **3**, 1154–1164.

32 H. Hu, S. Cai, H. Li, L. Huang, L. Shi and D. Zhang, In Situ DRIFTS Investigation of the Low-Temperature Reaction Mechanism over Mn-Doped Co₃O₄ for the Selective Catalytic Reduction of NO_x with NH₃, *J. Phys. Chem. C*, 2015, **119**, 22924–22933.

33 G. Gao, J.-W. Shi, Z. Fan, C. Gao and C. Niu, MnM₂O₄ microspheres (M = Co, Cu, Ni) for selective catalytic reduction of NO with NH₃: comparative study on catalytic activity and reaction mechanism via in situ diffuse reflectance infrared Fourier transform spectroscopy, *Chem. Eng. J.*, 2017, **325**, 91–100.

34 L. Wang, S. Zhang, Y. Zhu, A. Patlolla, J. Shan, H. Yoshida, S. Takeda, A. I. Frenkel and F. Tao, Catalysis and In Situ Studies of Rh₁/Co₃O₄ Nanorods in Reduction of NO with H₂, *ACS Catal.*, 2013, **3**, 1011–1019.

35 Y. Lou, L. Wang, Z. Zhao, Y. Zhang, Z. Zhang, G. Lu, Y. Guo and Y. Guo, Low-temperature CO oxidation over Co₃O₄-based catalysts: significant promoting effect of Bi₂O₃ on Co₃O₄ catalyst, *Appl. Catal., B*, 2014, **146**, 43–49.

36 X. Chen, X. Yang, A. Zhu, C. T. Au and C. Shi, In situ DRIFTS study during C₂H₄-SCR of NO over Co-ZSM-5, *J. Mol. Catal. A: Chem.*, 2009, **312**, 31–39.

37 M. C. Campa, D. Pietrogiacomi, C. Scarfiello, L. R. Carbone and M. Occhiuzzi, CoO_x and FeO_x supported on ZrO₂ for the simultaneous abatement of NO_x and N₂O with C₃H₆ in the presence of O₂, *Appl. Catal., B*, 2019, **240**, 367–372.

38 X. Xiao, S. Xiong, Y. Shi, W. Shan and S. Yang, Effect of H₂O and SO₂ on the Selective Catalytic Reduction of NO with NH₃ Over Ce/TiO₂ Catalyst: Mechanism and Kinetic Study, *J. Phys. Chem. C*, 2016, **120**, 1066–1076.

